

An Energy Management Unit for Predictive Solar Energy Harvesting IoT

Anuj Justus Rajappa¹ ^a, Adnan Sabovic¹, Burcu Celikkol³, Michiel Aernouts¹, Philippe Reiter¹,
Siegfried Mercelis¹, Peter Hellinckx², Jeroen Famaey¹

¹*IDLab, University of Antwerp - imec, Sint-Pietersvliet 7, 2000 Antwerp, Belgium*

²*IDLab, University of Antwerp, Groenenborgerlaan 171, 2020 Antwerp, Belgium*

³*OnePlanet Research Center, Bronland 10, Wageningen, Netherlands - 6708 WH*

{*anuj.justusrajappa, adnan.sabovic, michiel.aernouts, philippe.reiter, siegfried.mercelis, peter.hellinckx, jeroen.famaey*}@uantwerpen.be, *burcu.celikkol@imec.nl*

Keywords: EMU, Energy Management Unit, Energy Awareness, Energy Harvesting, Energy Aware Scheduler, Energy Prediction, Modular


Abstract: As the need for stand-alone energy harvesting devices increases, the alleviation of the ecological and economic impact of their production and maintenance is possible by increasing battery life while reducing needed battery capacity. However, the increasing energy requirements of far-edge Artificial Intelligence and long-range wireless transmissions in the Internet of Things threaten to demand ever-larger battery capacities for such remote devices. Dynamic adaptation of device operation based on harvestable energy – i.e., energy awareness – is a proposed solution and can be implemented using an energy management unit. Standardizing this unit as a separate, active electronic component with standardized drivers can simplify overall system development and benefit existing devices. Hence, we propose a novel interface that allows decoupling this unit from the rest of the system, independent of the power management unit in use. As a first step, we developed a prototype that uses the proposed interface to make existing, solar energy-based, third-party devices energy-aware with provisions to be cross-compatible with differing power management units. The prototype was evaluated using an air quality sensing device and improved the overall device’s transmission rate.

1 INTRODUCTION

Energy Harvesting (EH) embedded devices and systems are widely encouraged due to their self-sufficient nature and the flexibility they provide during the installation and maintenance (Chetto and Queudet, 2016). These devices usually harvest energy from unintentional ambient power sources (e.g., light, wind, heat, motion, etc.) (Shaikh and Zeadally, 2016), that are not under any artificial control for the intents of powering the device, and use the energy harvested for their normal operation. Due to the nature of their energy source, these devices have a low impact on the ecosystem compared to a purely battery-powered (Kang et al., 2013; Hamers, 2020) or grid-powered device (Yue et al., 2021).

Current Energy Harvesting Internet of Thing(s) (EH-IoT) devices often execute their tasks periodically with fixed time intervals (Kjellby et al., 2018; Bhusal et al., 2020; Kjellby et al., 2019; Ramson

et al., 2021), without taking their available energy budget into account. Consequently, this leads to power failures during periods with a low energy yield. On the other hand, excess energy is not optimally used during periods with a high energy yield. Having a large energy reservoir such as large capacity batteries or super capacitors might solve this issue, but that leads to higher costs, greater waste after end-of-life and larger form-factors (Shaikh and Zeadally, 2016). Ideally, devices should change their behavior based on their currently available energy, which will require energy-aware task scheduling (EATS) schemes for energy management (Babayo et al., 2017), where the device’s behaviour is altered by scheduling tasks based on the energy availability. For this purpose, researchers have developed energy-aware task scheduling algorithms for low power – and even battery-less – Internet of Things (IoT) (Sabovic et al., 2022; Delgado and Famaey, 2021). However, there are two variations of the same question whose answer is important to increase the EATS’s performance, “How much energy will be available after a certain time period?”

^a  <https://orcid.org/0000-0001-8167-9171>

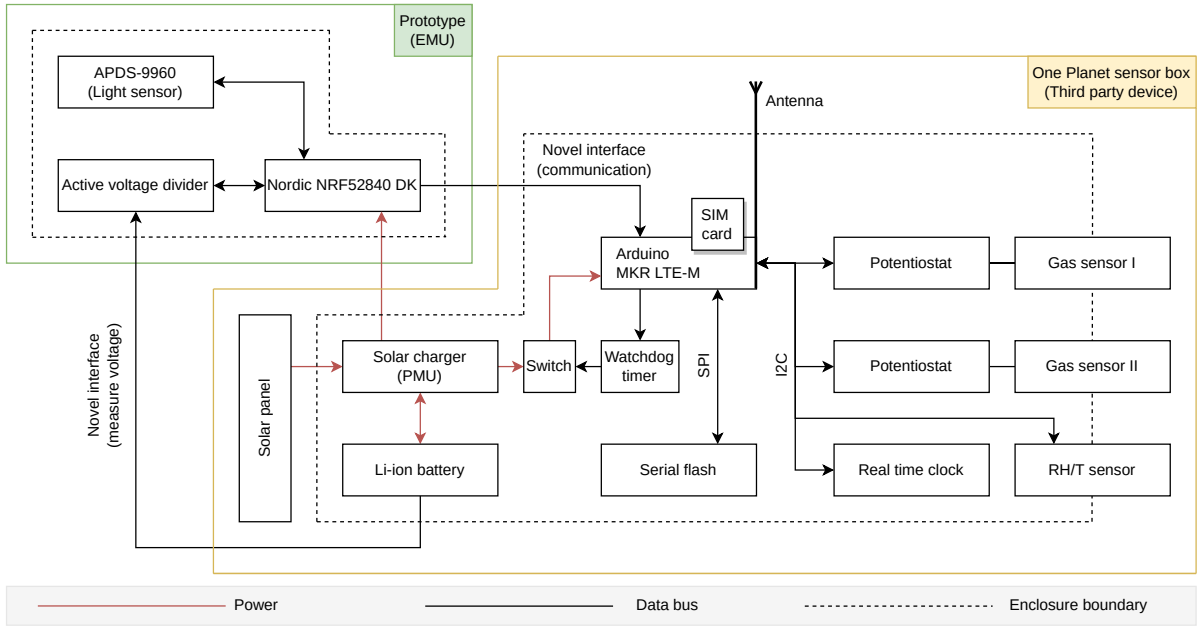


Figure 1: Overall system block diagram.

(first question) and “When will a certain amount of energy be available?” (second question). As both questions are concerned with future available energy, prediction algorithms, which allow the device to act proactively, are used to answer them (Shafik et al., 2018; Cammarano et al., 2016).

In this paper, unlike most of the current State of the Art (SotA) techniques discussed in Section 2, we focus on the second form of the question and answer it with an Auto-regressive Integrated Moving Average (ARIMA) based energy prediction algorithm. A simple EATS scheme uses the answer obtained (i.e. the timing information) to maximize the efficient utilization of harvested energy in a real EH-IoT device, which is usually not the case in current SotA systems as the implementations based on the ARIMA algorithm are often limited to simulation in this context (Ji et al., 2009; Tanha et al., 2021). The proposed predictive system is more adaptive and energy-efficient compared to periodic polling-based reactive techniques (Sabovic et al., 2022), which might require a backup battery for continuous operation (Anagnostou et al., 2018). Another novelty in our approach is that, unlike most of the current SotA systems that combine everything into one EH-IoT device, we separated the EATS scheme from the rest of the system by building it into a prototype (cf. Section 4) i.e. the energy management unit (EMU). This allows us to add energy awareness (i.e., EATS) to non-energy-aware third-party devices, through the proposed novel interface, with ease. This idea was validated using

OnePlanet sensor box (Hofman et al., 2022) equipped with Arduino as the third-party device and the corresponding overall system block diagram with only the significant connections is shown in Figure 1. The experimental setup used for validation is shown in Figure 5. In this paper, the role of EMU is associated with optimal control of power consumed by the device with respect to time, while the role of the power management unit (PMU) is associated with harvesting maximum power from the energy harvester.

Other differences in our approach from most of the current SotA are listed in Table 1. It includes handling power cycles (Rodriguez Arreola et al., 2022), due to energy shortages and additional overhead due to energy predictions, which are usually unaccounted by the current SotA energy prediction systems in EH-IoT.

2 RELATED WORK

Current SotA techniques extensively use energy prediction for answering the first question – i.e., “How much energy will be available after a certain time period ?” –, and use the energy information obtained to improve their task scheduling schemes. Statistical models, such as Exponentially Weighted Moving Average (EWMA) (Kansal et al., 2007), Weather Conditioned Moving Average (WCMA) (Recas Piorno et al., 2009) and similar (Noh and Kang, 2011; Dehwah et al., 2017), split a day into different time slots

Table 1: Difference between current SotA and our approach.

Current SotA approach	Our approach
Requires accumulated energy data from time slots older than at least a day (Kansal et al., 2007; Recas Piorno et al., 2009; Cammarano et al., 2012; Kosunalp, 2016; Stricker and Thiele, 2022; Yamin and Bhat, 2021) for prediction. Hence, non-volatile memory access to store day(s) old data and avoid data loss is required, if the power cycle (Rodriguez Arreola et al., 2022) is less than two days	Non-volatile memory access to store the time slot data for prediction is not required as it can be collected within a few minutes in the field. If the power cycle is less than a few minutes, then the required data can be augmented (cf. Section 3.2.2)
Overheads, such as the energy required to collect data in the field for prediction are not usually considered as prediction overhead (Cammarano et al., 2016; Stricker and Thiele, 2022; Yamin and Bhat, 2021)	Overheads associated with data collection in the field for prediction purposes are mostly accounted for and reported in Section 4 and Table 2
Accumulated solar energy (Yamin and Bhat, 2021; Stricker and Thiele, 2022) or harvested power (Cammarano et al., 2016; Kansal et al., 2007) is the prediction variable. This variable's present value is measured in an EH-IoT device using either some undisclosed circuitry (Yamin and Bhat, 2021) or solar current with or without voltage (Kansal et al., 2007; Dehwah et al., 2017), whose accuracy distortions due to PMU are not discussed. Training a prediction model with this variable often requires device-specific parameters, such as the characteristics of its solar panels or training data collected from a similar device, thus locking the trained model to those device parameters (Stricker and Thiele, 2022; Yamin and Bhat, 2021; Cammarano et al., 2016; Kansal et al., 2007). Hence, changing a device parameter might often require retraining the prediction model	Instantaneous solar irradiance is the prediction variable. The present value of this variable is measured using a dedicated light sensor, hence it is not affected by the PMU (cf. last paragraph, Section 5). Solar irradiance is the only variable used for training the prediction model. The model's predictions are integrated with time and device parameters, such as the efficiency of its solar panel, PMU, etc., for calculating the actual harvestable energy (cf. Equation 1). As these device parameters can be changed even during the run-time and are not involved in the prediction model's training process, it enables our prototype to be plugged into different devices without retraining the model
Long-term timekeeping (days) despite the power cycles (Rodriguez Arreola et al., 2022) is required for identifying time slots with respect to a day and for managing old data (Cammarano et al., 2012; Kansal et al., 2007; Stricker and Thiele, 2022; Yamin and Bhat, 2021)	Long-term timekeeping is not required as there is no need to identify any time slot with respect to a day. Data older than a few minutes are usually not required and are discarded
Prediction horizon is from short to long (minutes to days) (Cammarano et al., 2016)	Prediction horizon is very short (seconds to minutes)
Aperiodic sleep is not possible as the device needs to periodically collect the data for prediction (Cammarano et al., 2016; Kansal et al., 2007; Dehwah et al., 2017; Yamin and Bhat, 2021)	Aperiodic sleep is possible as the missing periodic data can be obtained using data augmentation (cf. Section 3.2.2)

and records the energy accumulated in those time slots during the present and previous days, which is later used for predicting future energy accumulation. PROfile Energy Prediction (Pro-Energy) (Cammarano et al., 2012) is based on data from previous days, but only typical days, which are characterized as sunny, rainy, cloudy or mixed, are stored. It analyzes the present-day weather condition and matches it with the closest profile, whose time slot data are then used for prediction. PROfile Energy prediction model with Variable Length Timeslots (Pro-Energy-VLT) (Cammarano et al., 2016) is based on Pro-Energy but the granularity of time slots for the profile are varied, based on the dynamics of power source. Improved PROfile Energy Prediction (IPro-Energy) (Muhammad et al., 2017) is based on Pro-Energy but the previous days recorded are based on how old they are rather than typical day characterization. It uses an additional parameter called ‘smarting factor’ that takes into account the rate of change of energy between the time slots. Enhanced Pro-Energy (Enhanced-Pro) (Deb and Roy, 2021) handles a previous day’s data similar to IPro-Energy but is also based on Pro-Energy. It adds two new parameters: the tuning factor, and the fine adjustment index to refine the accuracy.

Machine learning algorithms are also used for predicting energy (Stricker and Thiele, 2022; Yamin and Bhat, 2021). For instance, Q-learning-based solar energy prediction (QL-SEP) (Kosunalp, 2016) is an algorithm based on EWMA with an additional parameter called ‘daily ratio’, which is calculated using Q-learning. However, when dealing with short term energy predictions in solar-based EH low-power devices, statistical models are preferred to stochastic and machine learning models (Wahba et al., 2020; Bergonzini et al., 2009) due to their suitability in terms of accuracy and overhead.

3 ENERGY AWARE TASK SCHEDULER

This section describes our EATS, which consists of a task scheduling algorithm aided by the energy prediction algorithm. EATS is responsible for scheduling tasks associated with actions such as sense and transmit in the third-party device.

3.1 Task Scheduler

The prototype of EMU uses an energy-adaptive, cyclic-scheduler to schedule independent atomic tasks in the third-party device with the goal of max-

imizing the efficient utilization of harvested energy, thereby decreasing residual energy utilization from energy reservoirs. This is done in four steps. First, the prototype checks the battery voltage and proceeds to the next step if it is above the lower limit; else it rechecks after a predefined period. Second, the prototype selects the task to execute next. Third, it calculates the waiting period (cf. Section 3.2.3) and waits in sleep mode while collecting the energy required to execute this task. However, this step is skipped if the battery voltage is above the upper limit. Finally, it executes the task and the cycle repeats. Calculating the waiting period based on the required and harvestable energy is what makes the cyclic scheduler energy adaptive. It is done using energy prediction. This scheduler can also be replaced with more complex ones (Sabovic et al., 2022) (Delgado and Famaey, 2021) based on task priorities and dependencies, deadlines, etc.

3.2 Energy Prediction

A univariate time series forecasting technique is used by the prototype of EMU for energy prediction, using the non-seasonal ARIMA model (Tanha et al., 2021). The univariate being forecast is solar irradiance, whose historical time series data is used to train the model. Two functions, represented in Figure 2, were used to implement the ARIMA model in the prototype. Function 1 stores the observed data from the prototype and calculates the residuals (difference between observed and predicted value). Function 2 uses the observed data and residuals to predict the wait time for accumulating a certain amount of energy.

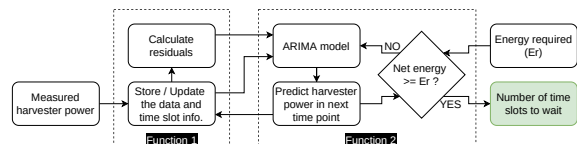


Figure 2: Implemented ARIMA model abstract.

The consecutive data samples observed and predicted have equal time intervals (sample period) between them, which can be used to split the time domain into multiple, equally spaced time slots. A sample collected at the end of a time slot also belongs to the beginning of the next time slot. The average of a particular samples belonging to the beginning and end of a particular time slot is assumed to be valid throughout that time slot; i.e., if S_{ir}^a and S_{ir}^c are the solar irradiance data measured at the beginning and end of a time slot, then the solar energy harvested per m^2 in that time slot is given by multiplying $\left(\frac{S_{ir}^a + S_{ir}^c}{2}\right)$ with the sample

period.

The observed data belonging to the beginning or end of a time slot are called lag values and it is the input to the Auto-regressive (AR) part of the ARIMA algorithm. The difference between the observed data and the corresponding prediction is called the residuals or lagged forecast errors and it is the input to the Moving Average (MA) part of the ARIMA algorithm. The values P,D and Q are parameters that define a ARIMA(P,D,Q) model, obtained after training the model using a custom framework in Python, that uses the `auto_arma()` function provided by ‘`pm-darima`’ (Taylor G. Smith, 2022) Python library. P represents the number of autoregressive terms, D represent the order of differencing required to convert a time series data from non-stationary to stationary, and Q is the number of residuals used by the prediction model. After training the model, an intercept value along with arrays of length P and Q containing coefficients corresponding to the AR and MA part of the prediction model are obtained. The P,D,Q values, coefficients and the intercept value are transferred to the embedded platform of the prototype, described in Section 4, and are used by the ARIMA model implemented in it using the C language. The number of lag values required by the model in the field for prediction is given by $\max(P+D,Q)$. To complete the training process within a reasonable time frame, the P,D,Q values were constrained to 10, thus the maximum number of lag values possibly required by the model would be 20. If each value consumes 4 bytes, the worst case memory consumption by the lag values will be 80 bytes.

3.2.1 Training and Testing

The dataset to train and test the model was collected using a custom setup (Anuj Justus Rajappa, 2022a; Anuj Justus Rajappa, 2022b), shown in figure 3, which includes a solar panel (Seed Studio, 2022) and APDS-9960 light sensor (BROADCOM, 2022) whose surfaces are placed on the same plane and as close to one another as possible, without obstructing the incoming light. The INA226 power sensor (Texas Instruments, 2022) was used to collect the solar panel’s open circuit voltage (V_{ocv}) and closed circuit current (I_{ccc}), while the light sensor was used to collect the solar irradiance data. An additional DHT22 temperature and humidity sensor (Aosong Electronics Co.,Ltd, 2022) was used to record the environmental data. The sensors were sampled every 200ms and logged. The setup was placed indoors, next to a curtain-less glass window facing south-west in Antwerp (Belgium) between August of 2021 and February of 2022. The total data col-

lected over around 120 days consumes approximately 2GB in memory and is publicly accessible (Anuj Justus, 2022). ARIMA(5,1,0) was obtained after training with the dataset obtained between 12-11-2021 to 15-01-2022 and testing was done with the dataset obtained between 24-01-2022 to 03-02-2022 due to their continuity in time. The performance of the model with the shortest prediction horizon (cf. Section 4) is shown in Figure 4a. The root mean square error (RMSE) for the prediction is around $7.99 \times 10^{-2} \frac{mW}{cm^2}$, which is two orders of magnitude less than the average operating range during daytime.

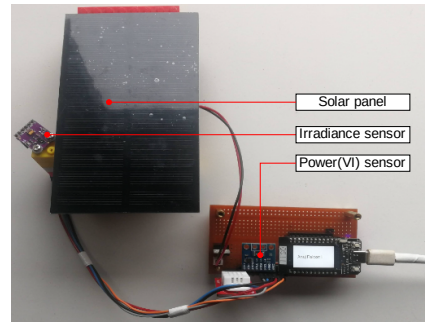


Figure 3: Custom setup for compiling historical dataset.

3.2.2 Deployment and Data Augmentation

Once the prediction model is trained and its parameters are transferred to the prototype of EMU, the past and present solar irradiance measurements from the field are required to predict the future value(s) of that variable, which is obtained using an APDS-9960 light sensor (BROADCOM, 2022) attached to the prototype. The sensor is disabled when not in use by issuing an I2C command to improve the prototype’s energy efficiency. The nature of the data required is time series; i.e., it must have a constant sampling period. Due to uncertainty in the energy availability, it is not possible to guarantee that the system will wake-up at regular intervals to collect the data for prediction. Besides, the wake-ups would also be costly in terms of energy consumption. So, whenever data is missing and is required for prediction, the required data is augmented with naive prediction using the previously observed data; i.e. using the previous observed data to fill the missing data. This also applies when the prediction horizon spans across more than one time slot. Assume the current time slot as T and the consecutive two time slots as T+1 and T+2. When predicting for the end of T+1, actual observed data until T is used as lag values. When predicting for the end of T+2, the lag value from the end of T+1 is required. Since it is in the future, the lag values are augmented by using

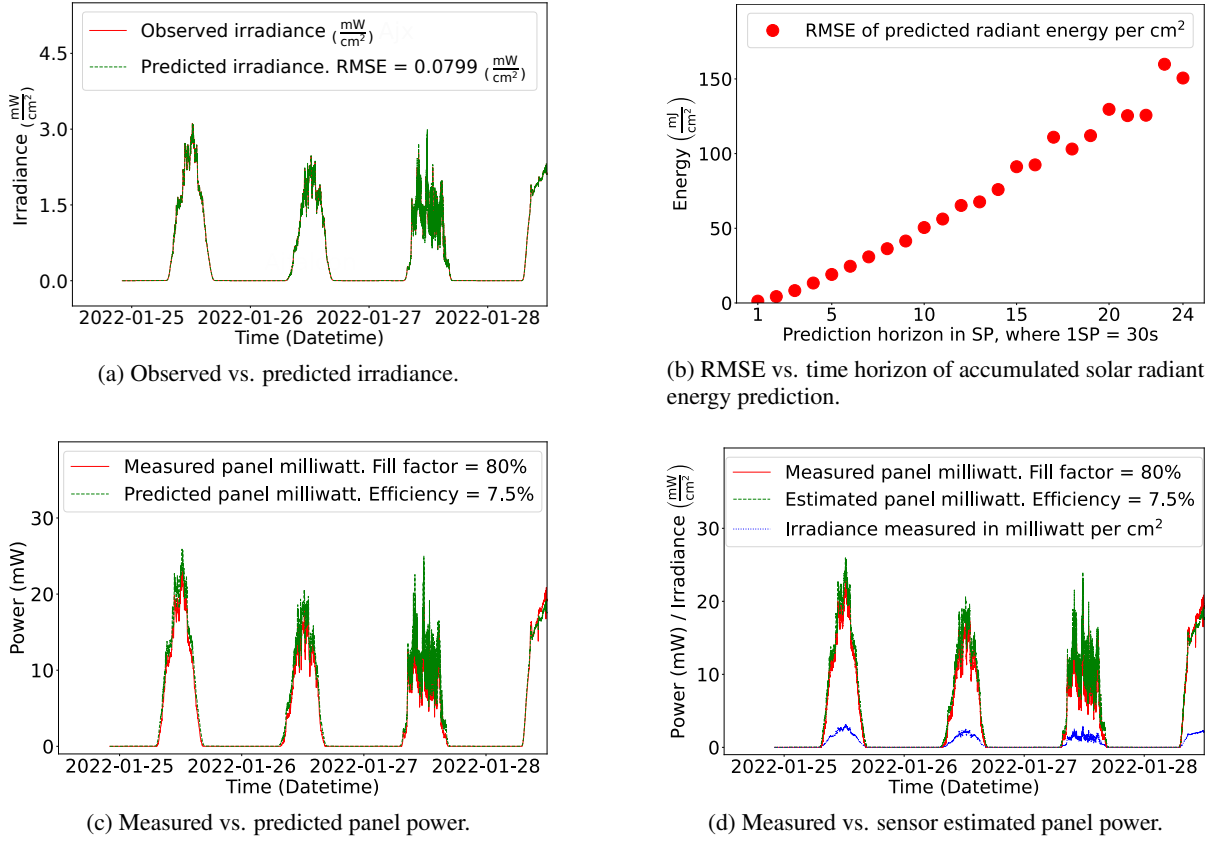


Figure 4: Analysis of the prediction and light sensor output.

the lag value from the end of time slot T . This will add to the prediction error such that it increases as the prediction horizon lengthens, as shown in Figure 4b.

3.2.3 Calculating Wait Time

Let T be the current time slot. $T+1, T+2, T+3, \dots$ represent the consecutive time slots in the future with sample period SP . Let IR_{T+n}^a and IR_{T+n}^z be the solar irradiance prediction for the beginning and end of the time slot $T+n$, where $n \in \mathbb{N}$. The harvested energy for that time slot ($Eh_{v_{T+n}}$) is calculated using the Equation 1, where PV_{area} is the surface area of the solar panel with efficiency PV_{eff} and PMU_{eff} is the efficiency of the PMU, which can be obtained from the datasheet of the solar panel and PMU, respectively.

$$Eh_{v_{T+n}} = \frac{IR_{T+n}^a + IR_{T+n}^z}{2} \times SP \times PV_{area} \times PV_{eff} \times PMU_{eff} \quad (1)$$

‘Function 2’ is responsible for calculating the wait time (cf. Figure 2). Let the measured quantity of energy required for a task to execute (Er) be input to

the function. The lowest value of w which will satisfy the Equation 2 is the function’s output, where $w \in \mathbb{N}$. The wait period is $w \times SP$. The graph showing the plot between the measured panel power using the custom setup (cf. Section 3.2.1) and predicted panel power (i.e. $IR^x \times PV_{area} \times PV_{eff}$, where IR^x is the irradiance predicted for the time point x) is shown in Figure 4c, where the efficiency of the panel was evaluated based on the obtained dataset and a typical fill factor value of 80% (Khanna et al., 2013; University of Washington, 2022) was chosen to assume the effects of maximum power point tracking (MPPT) in PMUs. The prediction’s RMSE is 1.35mW, which is an order of magnitude less than the average operating range during daytime.

$$Er < Eh_{v_{T+1}} + Eh_{v_{T+2}} + \dots + Eh_{v_{T+(w-1)}} + Eh_{v_{T+w}} \quad (2)$$

4 PROTOTYPE DESCRIPTION

The prototype of EMU is shown in Figure 5 and its block diagram is shown in Figure 1. It consists of

a Nordic nRF52840 development kit (Nordic Semiconductor, 2022) running in nRF only mode as the compute unit for running the prediction algorithms. Irradiance data is collected with the APDS-9960 light sensor, which communicates with the compute unit using I2C protocol. To monitor the energy reservoir, such as batteries, its voltage needs to be measured. However the range of voltage available at the battery terminal is incompatible with the range of voltage that can be input to the ADC unit of the prototype. Hence, a custom active voltage divider circuit was developed and was used to scale the battery voltage and bring it within the ADC input range. Electrical parameters of the prototype were measured with a Joulescope (Jetperch, 2022; Huybrechts et al., 2021) under different conditions, such as short-term time keeping with a high resolution timer (timer) versus a real-time clock (RTC), as shown in Table 2. A active max. scenario corresponds to the measurement made during the active states, when the sensor and EATS are in their maximum power consumption configuration. The Worst-case execution time (WCET) measured for the active states was around 240ms.

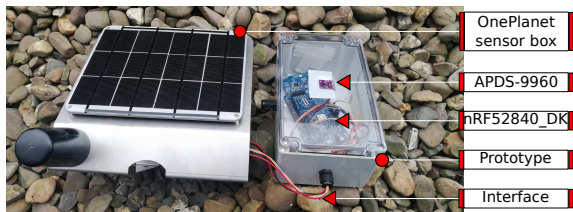


Figure 5: OnePlanet sensor box (left) and Prototype (right).

The prototype was interfaced with an air quality sensor from OnePlanet (Hofman et al., 2022), as shown in Figure 5. It consists of air quality monitoring sensors, a solar panel, a rechargeable lithium battery (J & A, 2022), a power management board, a processing and control unit from Arduino with on-board transceiver from uBlox, which is a LTE Cat M1 / NB1 and EGPRS cellular module to transmit the measurements at least once every 60 *minutes*. With our prototype, it was required to transmit a measurement at least once every 15 *minutes* i.e. to increase the performance by four times. The flow of the prototype’s firmware is shown in Figure 6. Function 2 (cf. Section 3.2.3) shown in Figure 2 is invoked to accumulate enough harvested energy only when the battery voltage is within its upper limit (4.1 V) and lower limit (3.3 V), which approximately marks the 100% and 30% states of charge, respectively (J & A, 2022). The last 30% of the battery is utilized as a reserve for handling worst-case and unexpected scenarios. Even during normal operation, it is not recommended to reach 100% depth of discharge, as it

Table 2: Electrical parameters of Prototype.

Scenario / Task	Power	Voltage
Sleep (timer0)	0.9mW	3.29
Active max. (timer0)	1.5mW	3.29
Sleep (rtc0)	35 μ W	3.29
Active max. (rtc0)	600 μ W	3.29

stresses the battery and worsens the cycle life (Battery University, 2022) and can cause the battery management system (BMS) to shutdown the power output. If the battery voltage is greater than the upper limit, it means enough energy is already available and can execute the next task. When battery voltage is below the lower limit, no task is executed and voltage is rechecked after a predefined period. WCET and Worst-case energy consumption (WCEC) of the tasks executed on the OnePlanet sensor box were not readily available but they are required to calculate the sample period and energy required in Function 2 (cf. Fig. 2). Hence, the WCET and WCEC of the tasks were measured using the Joulescope and the measurements are tabulated in Table 3. During sleep, the OnePlanet box consumes around 4.8mW at 3.29V. The execution time was calculated based on the energy consumption pattern. The worst case energy consumption is set as 0.13J for measurement and 14J for transmission (Tx), which includes some overhead to account for its consumption during sleep and operation of the prototype.

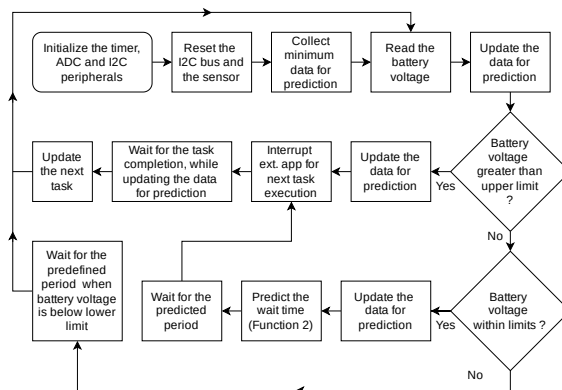


Figure 6: Flowchart of the prototype firmware.

4.1 Time Management

The sample period used by the prediction model was used to discretize the time domain and eliminate the complexity involved in calculating the time in the continuous time domain. Hence, all the execution times and wait times used by the firmware of the prototype of EMU are quantized with the quantum set as

the sample period (SP). This quantization of time domain can also reduce the number of wake-ups, certain routines and associated overheads by synchronizing the events to the points in the discrete time domain and therefore reducing the energy required. To increase the efficient utilization of the harvested energy, the device should be capable of executing tasks consecutively without delay. Hence, an average execution time of 61.8s, obtained from Table 3 for both the Tx and measurement tasks in the One-Planet sensor box, is considered for the sample period; i.e., 61.8s is halved and rounded to 30s is used as the sample period ($1SP = 30s$) by this prototype as it provides fine-grained control over the time domain during event scheduling. Lowering the sample period further might provide even finer control but increases the prediction overhead by increasing the iterations required to solve for w in Equation 2, sensor on-time, etc., thereby increasing the energy consumption as the sample period decreases.

Based on Table 3, the execution time for a measurement task is fixed as $1SP$ and the Tx task is fixed at $5SP$ and together they take $6SP$; i.e., 3 *minutes*. As there is a requirement to transmit at least every 15 *minutes* or $30SP$, the maximum waiting period affordable is $24SP$, which is the maximum prediction horizon used during evaluation by limiting the maximum value for w as 24 in Equation 2 during the evaluation. The maximum prediction horizon of $24SP$ (12 *minutes*) falls under very short to short prediction horizon. Since the sample period is the time slot period, the oldest data possibly required by the model would be sample period times the maximum number of lag values possibly required (cf. Section 3.2): i.e., $30s \times 20 = 10$ *minutes*.

4.2 Novel Interface

The interface of the prototype of EMU consists of three parts, as shown in Figure 1. One is to power our prototype, another to measure the voltage of the reservoir, and the third one is responsible for communication between the prototype and the third-party device. Currently, the communication between our prototype and the third-party device is done through edge-triggered interrupts (one per task). Only a minor firmware adaption was required in the third-party device to replace its old timer-based logic with interrupt-based triggers, which enables the device to receive alerts from our prototype when there is enough energy to measure or Tx. The current prototype can be interfaced to third-party devices with only solar panels as energy harvesters. From the current SotA EH-IoT systems, we couldn't identify a similar interface for

decoupling EMU from the rest of the system. Hence we consider this interface to be novel.

5 OBSERVATION AND DISCUSSION

An APDS-9960 light sensor was configured to operate with the value of 192_{10} in its ADC integration time (ATIME) register during the experiment. This causes the sensor to achieve maximum resolution of the irradiance measurement equivalent to a 16-bit ADC with the maximum count value of 65535_{10} , which takes almost 178ms of the execution time during the active states of the prototype of EMU. By changing the ATIME register value to 255_{10} , it only takes 2.78ms to conduct a measurement and the maximum count value will be lowered to 1025_{10} . Meanwhile the active state's WCET is reduced to around 14.3 ms with approximate power consumption of 2mW. This can significantly shorten the maximum energy consumption during an active state from around $144\mu J$ to around $29\mu J$ at the expense of the measurement's resolution.

The solar irradiance's trend can be roughly deduced with the battery voltage data available from the third-party backend server. As shown in Figure 7, it hits the maximum value and remains constant around the afternoon, when the solar irradiance is usually high relative to the rest of the day. The number of Tx and measurements along with the battery voltage for a single day (12-05-2022) is shown in Figure 7 with respect to time. Red bars indicate the number of Tx of the standalone third-party device, whereas green bars show the number of Tx when our prototype is plugged in. The standalone third-party device was programmed by the third-party to make 1 Tx every hour by default. The experiment was conducted on a sundeck facing north-east for 63 hours, between 11th to 13th of May, 2022 at Antwerp (Belgium). Hence, the standalone third-party device would have made 63 Tx. After plugging in our prototype to this device, we were able to achieve 694 Tx, which is an eleven-fold increase in Tx rate. Even if the default Tx rate was increased to the minimum observed rate of 6 Tx every hour, the performance improvement achieved would be around 80% increase in Tx rate. This can be attributed to EATS's dynamic optimization of the Tx rate compared to a constant Tx rate, as evident from Figure 7, for devices that use unintentional ambient power sources. Due to the cyclic nature of the scheduler, 1 Tx and measurement constantly consumes 8 active states, each consuming a maximum of around $144\mu J$ (cf. Section 4 and Table 2). With the RTC for

Table 3: Electrical parameters of OnePlanet sensor box.

Scenario / Task	Execution time	Electric current	Voltage	Charge
Boot (connection timeout)	69 s	65 mA	4.95 V	4.5 C
	80 s	36 mA	3.29 V	3 C
Boot (connected)	40 s	86 mA	4.17 V	3.4 C
1 measurement	1.75 s	14.2 mA	4.17 V	25 mC
(1 measurement) Tx failed	125 s	-	3.29 V	2.42 C
	71 s	-	4.17 V	1.13 C
(0 measurement) Tx	31 s	88 mA	4.17 V	2.73 C
(1 measurement) Tx	80.25 s	41 mA	4.17 V	3.3 C

time keeping, the energy consumed by the prototype during the experiment would have been around 3.32J per day (3.01J per day in sleep and around 0.31J per day in active state).

Overall, the battery voltage did not show a decreasing trend during evaluation. This means the battery’s state of charge is regularly replenished despite the increase in the operation rate, which can be attributed to the third-party device’s dynamic adaption to the harvestable energy due to the addition of the prototype. It also means that the system is now capable of detecting excess available energy, which can be effectively used by the third-party device for improving its quality of service (QoS) (Shafique et al., 2020) and energy efficiency. However, a decreasing trend in the battery voltage could have been noticed if the solar panel had lower panel wattage rating or the battery had lesser capacity, which opens the door for further optimization.

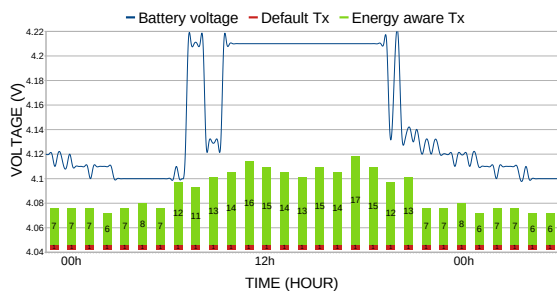


Figure 7: Number of Tx by default vs with the prototype.

The number of analog inputs required by the prototype for measuring the voltage at energy reservoir can increase if the third-party device uses multi-capacitor (Colin et al., 2018) or multi-battery based power source and could have a dedicated PMU to handle them. In such cases, the prototype is capable of working with no analog input by leaving the voltage checks to the third-party device, thus being able to operate without accessing the electrical data of the energy reservoirs by always waiting to acquire enough harvestable energy before executing a task. Currently,

the prototype’s interface requires one interrupt pin per task. Hence, increasing the number of tasks will increase the number of connections between the prototype and the third-party device. With this first implementation, there is no feedback when a task is executed. It is assumed to be executed after the WCET. Both these issues could be solved in the future using a standard communication protocol.

Energy harvested from unintentional ambient power sources can be difficult to monitor in an EH-IoT device deployed in a real environment, as conventional methods can be expensive in terms of energy. Harvested energy can be calculated by directly measuring the harvester power and integrating it with the sample period. Directly measuring power requires measuring voltage and electrical current, but the overheads can negate the overall benefit. For instance, using a shunt resistor-based passive electrical current measurement design consumes energy in and of itself, depending on the design and the resistor value. Another issue with direct power measurement is the access to the PMU. When plugging into third-party devices, this might not be easily possible. Even if possible, some PMUs (e-peas, 2022b; e-peas, 2022a) uses V_{ocv} of the solar panel to calculate the operating maximum power point voltage (V_{mpp}). Hence, synchronization is required so that direct power measurements aren’t made when the PMU is measuring V_{ocv} , which might require changing the PMU’s configuration, the interface and our prototype’s firmware depending on the exact PMU used by the third-party device. Otherwise, the PMU’s V_{ocv} measurement process can distort the direct power measurement causing its value to plummet to zero as the circuit is effectively broken during a V_{ocv} measurement.

In order to mitigate the disadvantages of the direct power measurement and, as solar panels were the only energy harvester being considered in this experiment, we used the light sensor to measure the incoming light energy in terms of irradiance (cf. Section 3.2.3). Using a separate sensor eliminates the need for tinkering with the PMUs of third-party devices and results

in a more independent interface. It allows us to disable this sensor when not in use or when the energy is low. The accuracy trade-off between directly measured and sensor-estimated panel wattage was studied using the custom dataset and was found to have an RMSE of 1.22mW, which is an order of magnitude less than the average operating range during daytime, as shown in Figure 4d (cf. Section 3.2.3), with raw solar irradiance data plotted in blue for reference.

6 CONCLUSION AND FUTURE WORK

We proposed a novel interface that brings energy awareness with ARIMA based short-term energy forecasting to non-energy aware EH-IoT devices and demonstrated its feasibility using OnePlanet sensor box. Our real world experiments with this system showed that the overall dynamically optimized Tx rate outperforms constant Tx rate based solution (cf. Section 5) and the efficient utilization of the harvested energy could be maximized, when compared to its standalone state. Instead of only increasing the Tx rate, the Tx power of the third-party device can also be increased with the prototype of EMU, which, can be more beneficial for exceedingly remote and indoor deployments. The prototype's ability to operate independently of the type of energy reservoir(s), and its ability to operate without retraining the prediction model even when the third-party device parameters change enable easy adaptation. During the evaluation period, the total energy overhead of our prototype (not just the prediction) built with commercial-off-the-shelf (COTS) components was estimated to be around 3.32J per day, with the majority of it consumed during sleep. This can be reduced by using more intentionally designed hardware (Zhang et al., 2011) and software. Future experiments for research purposes will benefit from increased evaluation periods, analyzing the impact of location and orientation of the third-party device, and adding an externally powered data acquisition (DAQ) system to monitor the environmental and in-system parameters affecting the system operation. It is also required to analyze the drift in the outputs from system components such solar panel, light sensor, PMU, etc., due to ageing or other factors and take these into account. In addition, the effect of spectral sensitivity on the error between measured and sensor-estimated panel Wattage needs to be analyzed.

ACKNOWLEDGEMENTS

Part of this research was funded by the Flemish FWO SBO S001521N IoBaLeT (Sustainable Internet of batteryless Things) project.

REFERENCES

- Anagnostou, P., Gomez, A., Hager, P., Fatemi, H., de Gyvez, J. P., Thiele, L., and Benini, L. (2018). Torpor: A power-aware hw scheduler for energy harvesting iot socs. In *2018 28th International Symposium on Power and Timing Modeling, Optimization and Simulation (PATMOS)*, pages 54–61.
- Anuj Justus (2022). Custom dataset collected for energy manager. <https://doi.org/10.5281/zenodo.7044952>.
- Anuj Justus Rajappa (2022a). Build a long-term daq system (part 1): The hardware design. <https://circuitcellar.com/research-design-hub/march-circuit-cellar-sneak-preview-2022/>. Last checked on Aug 19, 2022.
- Anuj Justus Rajappa (2022b). Build a long-term daq system (part 2): The software design. <https://circuitcellar.com/research-design-hub/april-circuit-cellar-sneak-preview-2022/>. Last checked on Aug 31, 2022.
- Aosong Electronics Co.,Ltd (2022). Dht22 (dht22 also named as am2302). <https://www.sparkfun.com/datasheets/Sensors/Temperature/DHT22.pdf>. Last checked on Aug 31, 2022.
- Babayo, A. A., Anisi, M. H., and Ali, I. (2017). A review on energy management schemes in energy harvesting wireless sensor networks. *Renewable and Sustainable Energy Reviews*, 76:1176–1184.
- Battery University (2022). Bu-808: How to prolong lithium-based batteries. <https://batteryuniversity.com/article/bu-808-how-to-prolong-lithium-based-batteries>. Last checked on Aug 19, 2022.
- Bergonzini, C., Brunelli, D., and Benini, L. (2009). Algorithms for harvested energy prediction in batteryless wireless sensor networks. In *2009 3rd International Workshop on Advances in sensors and Interfaces*, pages 144–149.
- Bhusal, H., Khatiwada, P., Jha, A., Soumya, J., Koorapati, S., and Cenkeramaddi, L. R. (2020). A self-powered long-range wireless iot device based on lorawan. In *2020 IEEE International Symposium on Smart Electronic Systems (iSES) (Formerly iNiS)*, pages 242–245.
- BROADCOM (2022). Apds-9960. <https://www.broadcom.com/products/optical-sensors/integrated-ambient-light-and-proximity-sensors/apds-9960>. Last checked on Aug 18, 2022.
- Cammarano, A., Petrioli, C., and Spenza, D. (2012). Pro-energy: A novel energy prediction model for solar and wind energy-harvesting wireless sensor networks. In *2012 IEEE 9th International Conference on Mobile*

- Ad-Hoc and Sensor Systems (MASS 2012)*, pages 75–83.
- Cammarano, A., Petrioli, C., and Spenza, D. (2016). Online energy harvesting prediction in environmentally powered wireless sensor networks. *IEEE Sensors Journal*, 16(17):6793–6804.
- Chetto, M. and Queudet, A. (2016). 3 - harnessing ambient energy for embedded systems. In Chetto, M. and Queudet, A., editors, *Energy Autonomy of Real-Time Systems*, pages 57–83. Elsevier.
- Colin, A., Ruppel, E., and Lucia, B. (2018). A reconfigurable energy storage architecture for energy-harvesting devices. *SIGPLAN Not.*, 53(2):767–781.
- Deb, M. and Roy, S. (2021). Enhanced-pro: A new enhanced solar energy harvested prediction model for wireless sensor networks. *Wireless Personal Communications*, 117(2):1103–1121.
- Dehwah, A. H., Elmetnani, S., and Claudel, C. (2017). Ud-wcma: An energy estimation and forecast scheme for solar powered wireless sensor networks. *Journal of Network and Computer Applications*, 90:17–25.
- Delgado, C. and Famaey, J. (2021). Optimal energy-aware task scheduling for batteryless iot devices. *IEEE Transactions on Emerging Topics in Computing*, pages 1–1.
- e-peas (2022a). Aem10330 solar energy harvesting. https://e-peas.com/wp-content/uploads/2021/08/Datasheet_AEM10330_solar_energy_harvesting_IC_REV1.1.pdf. Last checked on Aug 18, 2022.
- e-peas (2022b). Aem10941 solar energy harvesting. <https://e-peas.com/wp-content/uploads/2021/03/e-peas-AEM10941-datasheet-energy-harvesting.pdf>. Last checked on Aug 18, 2022.
- Hamers, R. J. (2020). Energy storage materials as emerging nano-contaminants. *Chemical Research in Toxicology*, 33(5):1074–1081. PMID: 32275142.
- Hofman, J., Nikolaou, M., Shantharam, S. P., Stroobants, C., Weijs, S., and La Manna, V. P. (2022). Distant calibration of low-cost pm and no2 sensors; evidence from multiple sensor testbeds. *Atmospheric Pollution Research*, 13(1):101246.
- Huybrechts, T., Reiter, P., Mercelis, S., Famaey, J., Latré, S., and Hellinckx, P. (2021). Automated testbench for hybrid machine learning-based worst-case energy consumption analysis on batteryless iot devices. *Energies*, 14(13).
- J & A (2022). J & a electronics li-ion cylindrical data sheet. <https://www.olimex.com/Products/Power/BATTERY-LIPO2200mAh/resources/JA18650-3.7V-2200mAh-Cell-Specification-150112.pdf>. Last checked on Aug 19, 2022.
- Jetperch (2022). Joulescope. <https://www.joulescope.com/>. Last checked on Aug 31, 2022.
- Ji, W., Chan, C., Loh, J., Choo, F., and Chen, L. (2009). Solar radiation prediction using statistical approaches. In *2009 7th International Conference on Information, Communications and Signal Processing (ICICSP)*, pages 1–5.
- Kang, D. H. P., Chen, M., and Ogunseitan, O. A. (2013). Potential environmental and human health impacts of rechargeable lithium batteries in electronic waste. *Environmental Science & Technology*, 47(10):5495–5503. PMID: 23638841.
- Kansal, A., Hsu, J., Zahedi, S., and Srivastava, M. B. (2007). Power management in energy harvesting sensor networks. *ACM Trans. Embed. Comput. Syst.*, 6(4):32–es.
- Khanna, A., Mueller, T., Stangl, R. A., Hoex, B., Basu, P. K., and Aberle, A. G. (2013). A fill factor loss analysis method for silicon wafer solar cells. *IEEE Journal of Photovoltaics*, 3(4):1170–1177.
- Kjellby, R. A., Cenkeramaddi, L. R., Frøylog, A., Lozano, B. B., Soumya, J., and Bhange, M. (2019). Long-range & self-powered iot devices for agriculture & aquaponics based on multi-hop topology. In *2019 IEEE 5th World Forum on Internet of Things (WF-IoT)*, pages 545–549.
- Kjellby, R. A., Cenkeramaddi, L. R., Johnsrud, T. E., Løvteit, S. E., Jevne, G., Beferull-Lozano, B., and Soumya, J. (2018). Self-powered iot device based on energy harvesting for remote applications. In *2018 IEEE International Conference on Advanced Networks and Telecommunications Systems (ANTS)*, pages 1–4.
- Kosunalp, S. (2016). A new energy prediction algorithm for energy-harvesting wireless sensor networks with q-learning. *IEEE Access*, 4:5755–5763.
- Muhammad, Qureshi, H. K., Saleem, U., Saleem, M., Pitsillides, A., and Lestas, M. (2017). Harvested energy prediction schemes for wireless sensor networks: Performance evaluation and enhancements. *Wireless Communications and Mobile Computing*, 2017.
- Noh, D. K. and Kang, K. (2011). Balanced energy allocation scheme for a solar-powered sensor system and its effects on network-wide performance. *Journal of Computer and System Sciences*, 77(5):917–932. PMECT 2009/ICCCN 2009.
- Nordic Semiconductor (2022). nrf52840 dk. <https://www.nordicsemi.com/Products/Development-hardware/nrf52840-dk>. Last checked on Aug 18, 2022.
- Ramson, S. R. J., León-Salas, W. D., Brecheisen, Z., Foster, E. J., Johnston, C. T., Schulze, D. G., Filley, T., Rahimi, R., Soto, M. J. C. V., Bolivar, J. A. L., and Málaga, M. P. (2021). A self-powered, real-time, lo-rawan iot-based soil health monitoring system. *IEEE Internet of Things Journal*, 8(11):9278–9293.
- Recas Piorno, J., Bergonzini, C., Atienza, D., and Simunic Rosing, T. (2009). Prediction and management in energy harvested wireless sensor nodes. In *2009 1st International Conference on Wireless Communication, Vehicular Technology, Information Theory and Aerospace & Electronic Systems Technology*, pages 6–10.
- Rodriguez Arreola, A., Verykios, T. D., Gurrola Navarro, M. A., and Calvillo Cortes, C. F. (2022). Federated time persistency in intermittently powered iot systems. *Journal of Systems Architecture*, 130:102667.
- Sabovic, A., Sultania, A. K., Delgado, C., De Roeck, L., and Famaey, J. (2022). An energy-aware task sched-

- uler for energy harvesting battery-less iot devices. *IEEE Internet of Things Journal*.
- Seed Studio (2022). Small solar panel 81x137mm 1.5w. <https://www.seeedstudio.com/1-5W-Solar-Panel-81X137.html>. Last checked on Nov 18, 2022.
- Shafik, R., Yakovlev, A., and Das, S. (2018). Real-power computing. *IEEE Transactions on Computers*, 67(10):1445–1461.
- Shafique, K., Khawaja, B. A., Sabir, F., Qazi, S., and Mustaqim, M. (2020). Internet of things (iot) for next-generation smart systems: A review of current challenges, future trends and prospects for emerging 5g-iot scenarios. *IEEE Access*, 8:23022–23040.
- Shaikh, F. K. and Zeadally, S. (2016). Energy harvesting in wireless sensor networks: A comprehensive review. *Renewable and Sustainable Energy Reviews*, 55:1041–1054.
- Stricker, N. and Thiele, L. (2022). Accurate onboard predictions for indoor energy harvesting using random forests. In *2022 11th Mediterranean Conference on Embedded Computing (MECO)*, pages 1–6.
- Tanha, S. N., Mim, S. A., Roy, P., and Razzaque, M. A. (2021). Prediction of energy harvesting in solar powered small cells networks. In *2021 3rd International Conference on Sustainable Technologies for Industry 4.0 (STI)*, pages 1–6.
- Taylor G. Smith (2022). pmdarima. <https://github.com/alkaline-ml/pmdarima>. Last checked on Aug 30, 2022.
- Texas Instruments (2022). Ina226 high-side or low-side measurement, bi-directional current and power monitor with i2c compatible interface. <https://www.ti.com/lit/ds/symlink/ina226.pdf>. Last checked on Aug 18, 2022.
- University of Washington (2022). Physics of solar cells. https://depts.washington.edu/cmditr/modules/opv/physics_of_solar_cells.html. Last checked on Nov 20, 2022.
- Wahba, M. A., Ashour, A. S., and Ghannam, R. (2020). Prediction of harvestable energy for self-powered wearable healthcare devices: Filling a gap. *IEEE Access*, 8:170336–170354.
- Yamin, N. and Bhat, G. (2021). Online solar energy prediction for energy-harvesting internet of things devices. In *2021 IEEE/ACM International Symposium on Low Power Electronics and Design (ISLPED)*, pages 1–6.
- Yue, H., Worrell, E., and Crijns-Graus, W. (2021). Impacts of regional industrial electricity savings on the development of future coal capacity per electricity grid and related air pollution emissions – a case study for china. *Applied Energy*, 282:116241.
- Zhang, Y., Shakhsheer, Y., Barth, A. T., Powell Jr., H. C., Ridenour, S. A., Hanson, M. A., Lach, J., and Calhoun, B. H. (2011). Energy efficient design for body sensor nodes. *Journal of Low Power Electronics and Applications*, 1(1):109–130.